Conf-9204158--8

PNL-SA--20350

DE92 013504

IRRADIATION EFFECTS ON THE ELECTROCHEMISTRY AND CORROSION RESISTANCE OF STAINLESS STEEL

S. M. Bruemmer
B. W. Arey
J. I. Cole
C. F. Windisch, Jr.

Received by OSTI
MAY 11 1992

April 1992

Presented at the
National Association of Corrosion Engineer
Corrosion '92
April 27 - May 1, 1992
Nashville, Tennessee

Work supported by
the U.S. Department of Energy
under Contract DE-AC06-76RLO 1830

Pacific Northwest Laboratory
Richland, Washington 99352

DISCLAIMER

This report was prepared as an account of work sponsored by an agency of the United States Government. Neither the United States Government nor any agency thereof, nor any of their employees, makes any warranty, express or implied, or assumes any legal liability or responsibility for the accuracy, completeness, or usefulness of any information, apparatus, product, or process disclosed, or represents that its use would not infringe privately owned rights. Reference herein to any specific commercial product, process, or service by trade name, trademark, manufacturer, or otherwise does not necessarily constitute or imply its endorsement, recommendation, or favoring by the United States Government or any agency thereof. The views and opinions of authors expressed herein do not necessarily state or reflect those of the United States Government or any agency thereof.

MASTER

DISTRIBUTION OF THIS DOCUMENT IS UNLIMITED

Corrosion 92: Corrosion of Materials in Nuclear Systems, Paper 92076

IRRADIATION EFFECTS ON THE ELECTROCHEMISTRY AND CORROSION RESISTANCE OF STAINLESS STEEL

S. M. Bruemmer, B. W. Arey, J. I. Cole* and C. F. Windisch, Jr.
Pacific Northwest Laboratory, Richland, WA
*Washington State University, Pullman, WA

Abstract

Nickel-ion irradiation at 500°C is shown to have a strong effect on the surface electrochemistry and intergranular corrosion of stainless steel. Measured current densities in a 1N H_2SO_4 solution at room temperature are increased at active-passive, passive, and transpassive potentials. Irradiation effects on the current decay behavior and susceptibility to intergranular corrosion were similar for a microcrystalline, fine-grained stainless alloy and for a very large-grained stainless steel. Radiation-induced segregation at the surface is believed to promote higher currents, whereas segregation at grain boundaries prompts intergranular attack. Analytical electron microscopy measurements reveal silicon enrichment and chromium depletion at internal interfaces in irradiated specimens. Silicon enhances dissolution at transpassive potentials, whereas chromium depletion does the same at active-passive and passive potentials.

Introduction

Irradiation-assisted stress corrosion cracking (IASCC) refers to environment-induced cracking of materials exposed to ionizing radiation. IASCC is a current concern for iron- and nickel-base stainless alloy core components in light-water reactors. Cracking susceptibilty is observed after a critical fluence of ~5 x 10^{20} n/cm^2 (1 dpa) in high-temperature (288°C) water environments. The morphology of cracking is intergranular (IG), similar in appearance to classical sensitization-induced IGSCC. Although the exact mechanism controlling IASCC is not known, irradiation exposure impacts a wide range of parameters that may promote SCC. The most important of these are:

(1) radiation-induced changes in grain boundary chemistry leading to enhanced reactivity/impaired passivity at the crack tip,
(2) radiation-induced changes in the reactor water making the corrosive environment more aggressive, and
(3) radiation-induced changes in deformation processes altering crack-tip mechanics.

Grain boundary chemistry is a primary cause of IG embrittlement in many structural materials including stainless alloys.[1] This observed behavior,

and the fact that neutron irradiation causes significant chemistry changes at interfaces, suggests that radiation-induced segregation (RIS) may be a primary cause for IASCC. RIS has been used to explain the effect of fluence on cracking based on impurity segregation[2,3] or Cr depletion[4,5] at grain boundaries. A recent review by Andresen et al.[4] gives a detailed discussion of IASCC processes and phenomena.

The current work examines the influence of irradiation on the electrochemical response and corrosion behavior of stainless steel at active-passive, passive, and transpassive potentials. Ion-irradiated fine- and large-grained materials are evaluated by static and potentiodynamic tests. Microstructures and local microchemistries are measured before and after irradiation using analytical electron microscopy. Radiation-induced segregation of solutes is compared to observed changes in stainless steel electrochemistry and susceptibility to IG corrosion.

Experimental Procedure

Materials

Nickel-rich, low-carbon 304-type stainless steel was sputter deposited as 0.13-mm thick foil for ion-irradiation studies. Deposit composition (in wt%) was Fe-21Ni-18.6Cr-1.5Mn-0.7Si-0.07P-0.0005C. The sputter-deposited material was heat treated to produce a grain size (~0.3 μm) several times smaller than the ion damage depth. Heat treatment temperature (750°C) was 250° higher than the irradiation temperatures so that thermally induced grain growth would not occur during irradiation. A more detailed description of the fine-grained (FG) material production is given elsewhere.[6,7] A large-grain (LG), commercial-purity 304 SS material was also examined. The bulk composition of this heat was measured (in wt%) as 0.06 C, 18.48 Cr, 8.75 Ni, 0.2 Mo, 1.7 Mn, 0.39 Si, 0.065 N, 0.013 P and 0.012 S. Specimens were solution annealed (SA) at 1325°C for 1 hour, cooled to 1100°C and water quenched to produce a "macrocrystalline" grain size of ~400 μm with no evidence of second phase (e.g., carbide) precipitates in the matrix or along grain interfaces.

Ion Irradiation

A 2-MeV tandem accelerator was used to generate a beam of 5 MeV Ni^{2+} ions for ion bombardment to minimize compositional and structural effects of the embedding atoms. Three-mm-diameter discs punched from the FG or LG materials were lightly abraded and given an electrochemical polish (in a solution of 5% perchloric acid in methanol at -35°C) prior to ion bombardment. Disc specimens were mounted in a vacuum chamber and irradiated to a damage level of 5 dpa. The total damage depth was ~1.2 μm. Specimens were irradiated under vacuum (<5×10^{-6} Pa) at a dose rate of 3×10^{-3} dpa/s.

Grain Boundary Composition Measurements

Elemental compositions across grain boundaries were measured using a Philips EM400T TEM/STEM or a Vacuum Generators HB501 STEM, both equipped with an energy dispersive X-ray spectrometer (EDS). Sample

preparation for transmission electron microscopy (TEM) was done by electrochemical jetting and polishing in a 5 vol% perchloric acid-methanol solution cooled to -40°C. EDS analysis was obtained using a 10-nm incident electron probe in the EM400T and a 2-nm probe in the HB501. Foil thickness in analysis regions was from 50 to 100 nm so that through-thickness resolution was generally less than 20 nm for the EM400T and less than 4 nm for the HB501.

Electrochemical and Corrosion Tests

The 3-mm-diameter disks described above were used for static or potentiokinetic exposures in 1N H_2SO_4 at 23°C. A region, 2-mm in diameter, was isolated for anaysis by masking off the outer edge of the disks. Potentiodynamic polarization curves were run using a PAR 273 potentiostat at a scan rate of 1 mV/s. These curves identified the potential regions of interest for constant-potential step tests. In each case, specimens were held for 10 s at a potential 0.1 V cathodic to the open circuit potential and then were directly stepped to the anodic test potential. Current density was monitored versus time via computer (in 0.03-s time increments) and continuously by strip chart recorder to a total exposure time of 1000 s. A 3-electrode system was used for all electrochemical measurements with a saturated calomel electrode (SCE) as the reference electrode. The degree and morphology of surface attack was documented after exposures by scanning electron microscopy (SEM). Care was taken to ensure that preferential attack did not occur near the edge of the mask region. Edge effects were observed if cathodic pretreatment times or the anodic exposure times were significantly increased.

Results and Discussion

Irradiation Effects on Microstructure and Microchemistry

Ion irradiation at 500°C produces a significant increase in the dislocation density of both the FG and LG materials. Primary damage is in the form of dislocation loops with no indication of radiation-induced precipitation under these irradiation conditions. A limited number of small voids (~10 nm in diameter) were detected in the LG 304 SS, while no voids were observed in the FG, Ni-rich 304 SS. The higher Ni and P levels in the FG material may delay the nucleation of voids to a higher dose in comparison to the LG material.

Damage levels of 5 dpa sharply altered the composition in the grain boundary region of the FG material.[4,6,7] Enrichment of Ni and Si as well as depletion of Cr and Fe was identified at most boundaries in the Ni-rich 304 deposit. No segregation or depletion of solutes was observed for specimens in the unirradiated condition, i.e., after the 750°C/1-h heat treatment. Grain boundary compositions of major (Fe, Ni, and Cr) and minor (Si) alloying elements were comparable to levels measured near the center of individual grains in irradiated alloys.

Irradiation-induced segregation was localized to a narrow region surrounding grain boundaries. Only EDS spectra generated within 5 nm of

the grain boundary revealed any composition difference from the matrix. Compositions measured at distances greater than ~10 nm from the interface were comparable to those taken near the center of the grain. The measured and interpolated compositions for Fe, Ni, Cr, and Si at grain boundaries are summarized in Table 1. A typical depletion profile for Cr is illustrated in Figure 1.

Phosphorus was not observed at grain boundaries even though present at high levels (0.06 wt%) in the bulk. This suggests that phosphorus enrichment is relatively small and is highly localized at interfaces. If phosphorus is only enriched within the boundary plane (i.e., over ~ 2 atom spacings as for equilibrium segregation), then a few percent phosphorus may be present, but below STEM-EDS detectability.

No measurements of RIS at grain boundaries have been made on the LG stainless steel. Because of the extremely large grain size, it is difficult to find a sufficient number of high-angle grain boundaries for AEM analysis. RIS model predictions[8] suggest that segregation of the major alloying elements (Fe, Ni, Cr, and Si) should be similar between the two materials. The higher Ni content in the FG material would tend to increase RIS slightly, but grain size differences should not have a strong effect.

Electrochemical Behavior of Unirradiated Materials

Potentiokinetic polarization curves for the FG Ni-rich stainless alloy and for the LG stainless steel are presented in Figure 2. Both show classical active-passive behavior with corrosion potentials (E_{corr}) of about -0.3 V and passive regions extending from about -0.1 V to 0.8 V. Examination of multiple polarization curves suggests that under the same conditions, LG specimens exhibit a lower E_{corr}, active-to-passive, and passive-to-transpassive transition potentials than the FG specimens. However, these differences were quite small, less than 0.02 V. Peak active and minimum passive currents were also comparable between FG and LG materials.

Potential step tests were performed at various potentials ranging from the active-passive to the transpassive region. A consistent change in current density with time response was observed with increasing potential as illustrated in Figure 3(a) for FG specimens. Currents decay rapidly with time at all potentials due to film formation. Steeper slopes are seen at passive potentials (-0.1 to 0.4 V) indicating the formation of a thin, protective film. As the potential is increased, curves are offset to higher current densities suggesting the growth of a thicker, less protective film.[9] A similar trend is seen for the LG specimens in Figure 3(b) with current decay curves shifting upward as higher anodic potentials are imposed. Step tests are in good agreement with the potentiodynamic polarization curves in Figure 2. To illustrate this, the measured current densities after 100 s are plotted as a function of potential in Figure 4.

Only FG specimens exposed to static tests at 1.025 V revealed any localized attack. Slight grain boundary attack was observed after the 1000-s exposure. The increase in current density with time for this specimen after ~250 s (Figure 4a) suggests the onset of IG corrosion. At 1.0 V, a light grain-to-grain etching is seen, but no IG attack. LG specimens did not exhibit localized corrosion at any potential after 1000

s exposures. However, long-time tests (>1 h) at 1.0 V did show IG attack of both the FG and LG materials.

Irradiation Effects on Electrochemical Behavior

Specimens from both heats were ion-irradiated to a dose of 5 dpa at 500°C, and potential step experiments were conducted at passive and transpassive potentials. Current-time response curves were found to be higher for the irradiated versus unirradiated specimens in all cases except for the FG specimen tested at -0.1 V. Results are documented in Figures 5 and 6 for FG and LG specimens, respectively. Irradiated specimens exhibit higher initial currents that decay at a similar rate as that for the unirradiated specimen. As a result, most curves appear to be simply offset from one another, with the irradiated curve moved upward to higher currents or shifted to longer times.

As noted above, FG specimens did not show an irradiation effect at -0.1 V. Irradiated and unirradiated current decay curves lie right on top of one another (Figure 5a). This potential showed the most passive response in the unirradiated condition and is near the active-passive range illustrated in Figures 2 and 4. Step tests on FG specimens at a more anodic passive potential (0.4 V, Figure 5b) indicated a large influence of irradiation. Current densities measured on the irradiated specimen are about 4X greater initially and the difference increases with time to >10X. All grain boundaries are attacked in the irradiated FG specimen, while only crystallographic etching is noted for the unirradiated specimen. Surprisingly, SEM micrographs also revealed similar localized corrosion at boundaries in the irradiated specimen at -0.1 V. Intergranular attack was not observed for any unirradiated specimen at potentials of 1.0 V or less.

The LG material was also tested at passive (-0.1 and 0.4 V) potentials and at a potential in the active-passive region (-.25 V). Potentials near the active-passive transition revealed significantly higher current densities after irradiation (Figures 6a), while the 0.4 V specimens showed a somewhat smaller effect (Figure 6b). Irradiation prompted some localized corrosion at passive potentials in the LG 304 SS. Intergranular corrosion was detected at all anodic potentials with the severity of attack decreasing with increasing potential. Occasional fine pits were present on LG specimens after the -0.1 and 0.4 V exposures. Attack appeared to be associated with surface scratches. Unirradiated LG specimens also experienced some pitting at these potentials. Pitting was not observed on the FG specimens at any potential.

Irradiation also modified the current response during step tests at transpassive potentials. Two potentials were examined in the FG material, 0.9 V (Figure 5a) and 1.025 V (Figure 5b). Currents for irradiated specimens were greater at both potentials. Slight IG grooving can be seen at 0.9 V, while the most severe attack at any potential is present after 1000 s at 1.025 V. Attack at 0.9 V is less than at -0.1 or 0.4 V and much less than at 1.025V. Very slight IG grooving was detected on unirradiated FG specimens at 1.025 V. LG specimens did not exhibit localized attack at a transpassive potential of 1.0 V. Currents were higher after irradiation (Figure 6b), but much longer exposure times were required for IG attack.

Mechanisms Controlling Irradiation Effects

Irradiated stainless steels exhibited higher currents and IG attack at passive and transpassive potentials. A likely cause for these effects is RIS due to Ni-ion bombardment. Grain boundaries in the FG Ni-rich, stainless alloy were found to be depleted in Cr and enriched in Si after irradiation. Chromium content has been shown to control electrochemical behavior of Fe-Ni alloys.[10-13] The passive nature of the film increases dramatically with Cr content, as does the potential range over which the film is stable. Lower Cr alloys or locally depleted regions would exhibit higher dissolution rates and thicker, less passive films. The observation of IG corrosion at active-passive and passive potentials is consistent with a Cr depletion mechanism. Inazumi et. al.[14] also identified grain boundary attack after electrochemical potentiokinetic reactivation (EPR) tests on neutron-irradiated (9 dpa at 420°C) stainless steel specimens. The EPR test scans a potential range through the passive-to-active region and is sensitive to Cr depleted regions below about 13.5%.[15]

The effect of chromium on anodic currents reverses at transpassive (>0.8 V) potentials, i.e. measured currents tend to decrease, not increase, as the Cr level is reduced. Thus, the higher currents and intergranular corrosion prompted by irradiation at 0.9, 1.0, and 1.025 V are not caused by Cr depletion. At these high oxidizing potentials, impurities such as P and Si accelerate dissolution. The influence of P has been more extensively studied,[16,17] but Si also promotes attack.[18,19] Since Si concentrations of up to 10% have been measured at grain boundaries in irradiated FG alloys, RIS of this element may be responsible for the accelerated IG corrosion. Phosphorus may play a role, but its segregation level was below detectibility in AEM.

The potential step test data show a dependence on irradiation. The effect of irradiation, however, appears to involve only shifting the log-current-versus-log-time plots to higher currents. The basic shapes of the curves are similar for non-irradiated and irradiated samples. This result suggests that the mechanism of film formation is similar for the stainless alloys with and without irradiation. Furthermore, it indicates that irradiation only effects the time/current necessary for the onset of film formation.

Measured current responses were consistent with those observed on other film-forming materials.[20,21] This is particulary the case in the passive region where clearly defined linear segments in the log-log plots were observed. (See Figures 3a and 3b) These linear segments follow a rate relation of:

$$\log i = \log k - m \log t \qquad \text{or} \qquad i = kt^{-m}$$

where m is a constant whose value indicates the mechanism of film formation, and k is a constant that is expected to be a function of the identity and structure of the surface film.[19] The parameter m has been shown to vary between 0.5 and 1.0 for the passivation of both iron and carbon steel. In this work, m was found to take on values in this range for many of the time segments and applied potentials studied.

Because the basic shape of the log-log plots are similar for non-irradiated and irradiated samples, it appears that the influence of irradiation is on the parameter k and not m. The effect of irradiation on k is consistent with RIS *at the surface* prompting a higher initial current and delaying passivation. Removal of this surface RIS region (several nm in depth) should be quite rapid and could simply offset the current decay curves to slightly longer times, thus increasing k.

Comparing the potential step test data for the FG (Figure 5) and LG (Figure 6) specimens indicates that RIS to *grain boundaries* is not controlling the increased current response for the irradiated samples. If grain boundary attack was a dominant factor, a much smaller irradiation effect would be expected for LG versus FG specimens, since the grain boundary area intersecting the surface in the LG alloy is orders of magnitude less than that for the FG steel.

The present observations do not preclude an influence of radiation-induced defects in the matrix on the electrochemical behavior. However, no indication of localized pitting was seen that might be associated with the dislocation microstructure produced by ion irradiation. Inazumi et. al.[14] observed localized attack on grain faces after EPR tests on their neutron-irradiated stainless steel specimens. Transgranular attack was ascribed to Cr depletion at small voids and dislocation loops in the matrix. Such attack was not seen in the present study probably because of the less severe irradiation exposure and reduced RIS to matrix defects. Electrochemical tests are continuing on specimens irradiated to lower levels of damage where RIS is considerably reduced.

Conclusions

Nickel-ion irradiation has a strong effect on the surface electrochemistry of stainless alloys in a 1N H_2SO_4 solution at room temperature. Irradiated specimens show higher current densities at all passive and transpassive potentials examined. Intergranular corrosion is observed for irradiated specimens at active-passive, passive, and transpassive potentials. Electro-chemical response and IG corrosion is believed to be caused by RIS of impurities and depletion of chromium at the surface and at grain boundaries. Irradiation-induced Si enrichment and Cr depletion is measured at grain boundaries. Silicon segregation promotes attack at transpassive potentials, whereas chromium depletion does the same at passive potentials.

Acknowledgements

Contribution of L. A. Charlot for AEM analysis is gratefully acknowledged. This work was supported by the Materials Sciences Branch, Office of Basic Energy Sciences, under Contract DE-AC06-76RLO 1830 with Pacific Northwest Laboratory which is operated by Battelle Memorial Institute.

References

1. S. M. Bruemmer, *Grain Boundary Chemistry and Intergranular Fracture*, Mat. Sci. Forum, Vol. 46, eds. G. S. Was and S. M. Bruemmer, Trans Tech Publ., Switzerland, 1989, p. 309.

2. A. J. Jacobs, R. E. Clausing, L. Heatherly and R. M. Kruger, *Proc. 14th Int. Sym. Effects of Radiation on Materials*, American Society for Testing and Materials, Andover, MA, 1988.

3. A. J. Jacobs, R. E. Clausing, M. K. Miller and C. Shepard, *Proc. 4th Int. Sym. Environmental Degradation of Materials in Nuclear Power Systems - Water Reactors*, eds. D. Cubicciotti and G. J. Theus, National Association of Corrosion Engineers, Houston, TX, 1990, p. 14-21.

4. P. L. Andresen, F. P. Ford, S. M. Murphy and J. M. Perks, ibid, p. 1-83.

5. S. M. Bruemmer, L. A. Charlot and E. P. Simonen, *Proc. 5th Int. Sym. Environmental Degradation of Materials in Nuclear Power Systems - Water Reactors*, ed. E. P. Simonen, American Nuclear Society, Monterey, CA, 1991.

6. S. M. Bruemmer, L.A. Charlot and M. D. Merz, J. Nucl. Mat., 1991, in press.

7. S. M. Bruemmer, L. A. Charlot, B. W. Arey and M. D. Merz, *Irradiation Effects on Grain Boundary Chemistry of Austenitic Stainless Steels*, Final Report, Research Project 2680-09, Electric Power Research Institute, Palo Alto, CA, 1991, in press.

8. E. P. Simonen, L. A. Charlot and S. M. Bruemmer, Corrosion 91, Paper 39, National Association of Corrosion Engineers, 1991.

9. K. Sugimoto and S. Matsuda, Mat. Sci. Eng., 42, 1980, 181.

10. K. Osozawa and H.-J. Engell, Corros. Sci., 6, 1966, 389.

11. V. Chihal, Zasncita Metallov, 4 (6), 1968, 563.

12. K. Kushiya, K. Suginoto and T. Enima, J. Jpn Inst. Metals, 42, 1978, 1109.

13. V. Jagannathan, T. A. Mozhi, W. A. T. Clarke and B. E. Wilde, Corros. Sci., 27 (6), 1987, 555.

14. T. Inazumi, G. E. C. Bell, E. A. Kenik and K. Kiuchi, Corrosion J., 46 (10), 1990, 786.

15. S. M. Bruemmer, L. A. Charlot and B. W. Arey, Corrosion J., 44 (6), 1988, 328.

16. C. L. Briant, Metall. Trans., 16A, 1985, 2061 and 18A, 1987, 691.

17. S. M. Bruemmer, E. P. Simonen and L. A. Charlot, ibid 3, 14-1.

18. J. S. Armijo, *Effects of Impurity Additions on the Intergranular Corrosion of High-Purity Fe-Ni-Cr Alloys*, General Electric Report, GEAP-5047, 1966.

19. K. T. Aust, Trans. AIME, 245, 1969, 2117.

20. W. Kozlowski and J. Flis, Corros. Sci., 28, 1988, 787.

21. D. D. Macdonald and B. Roberts, Electrochim. Acta, 23, 1978, 557.

Table 1

Measured Elemental Concentrations (wt%) in FG Material Irradiated to 5 dpa at 500°C

Element	Matrix Minimum-Maximum	Grain Boundary Minimum-Maximum	GB Average
Cr	17.3 - 18.5	9.6 - 15.7	12.2
Fe	60.4 - 62.5	54.3 - 59.5	57.4
Ni	20.3 - 22.1	23.5 - 29.5	27.1
Si	0.4 - 0.6	1.9 - 4.5	3.5

A total of 12 high-angle boundaries were analyzed. Beam dilution effects have been accounted for in the reported grain boundary concentrations as described in reference 7.

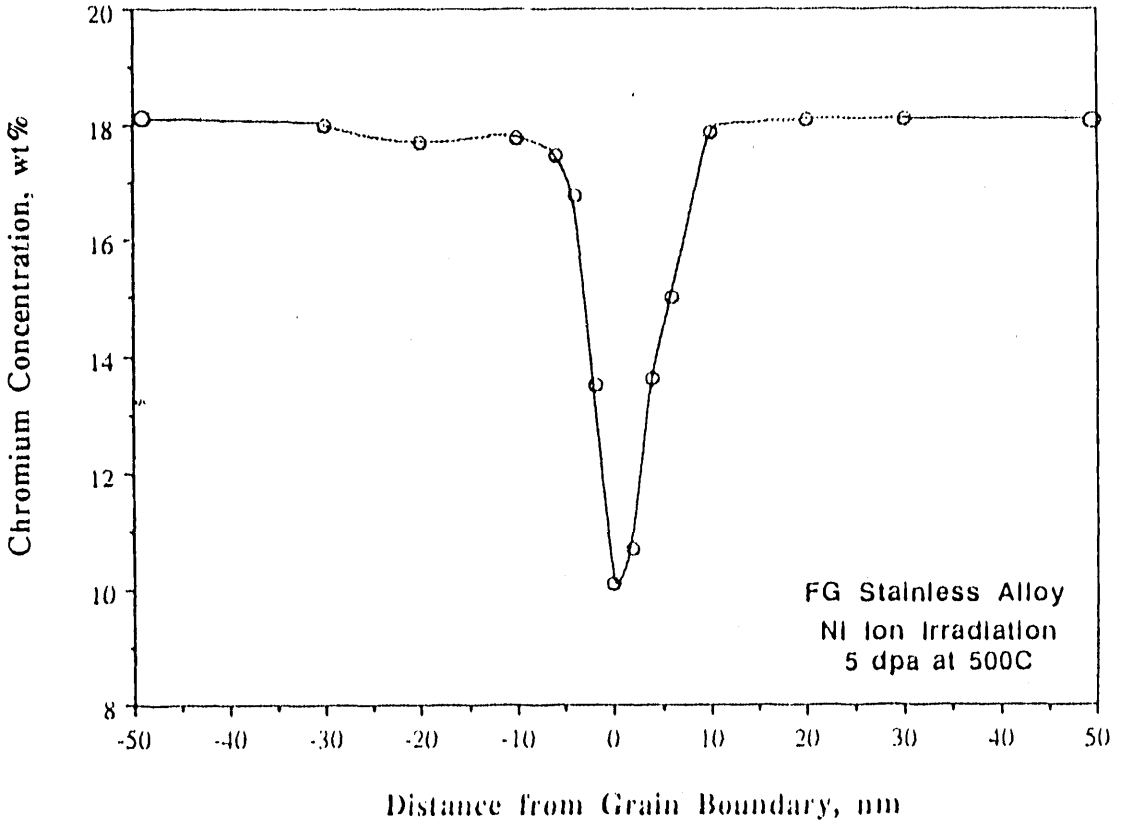

Figure 1. Measured Cr Depletion Profile for Ion Irradiated FG Material.

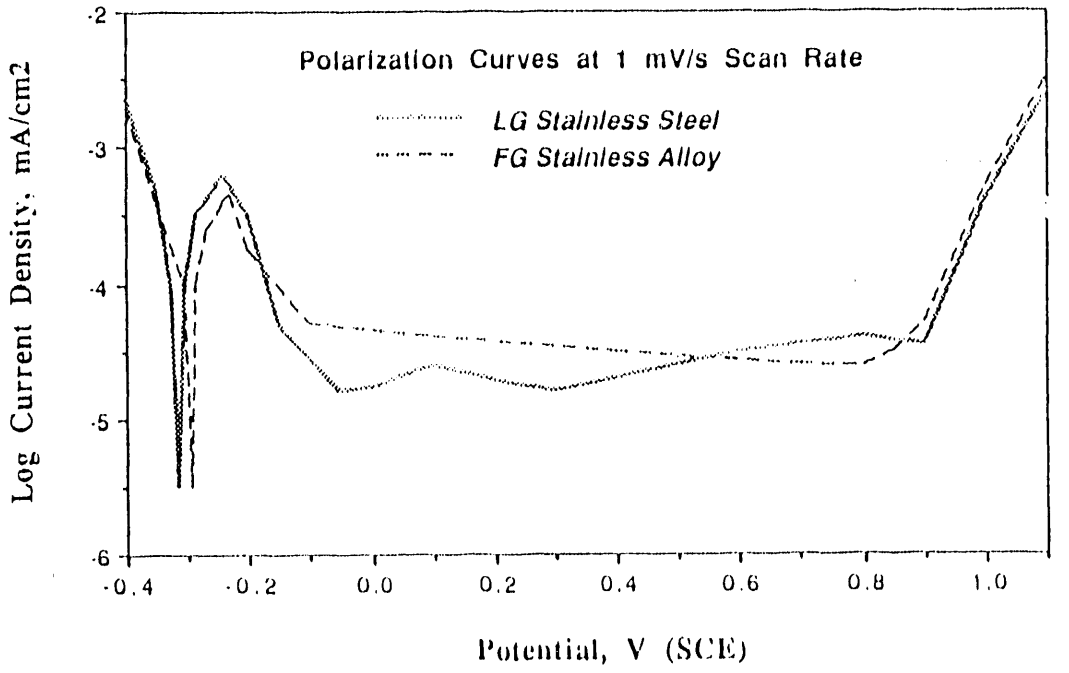

Figure 2. Polarization Curves for FG and LG Materials.

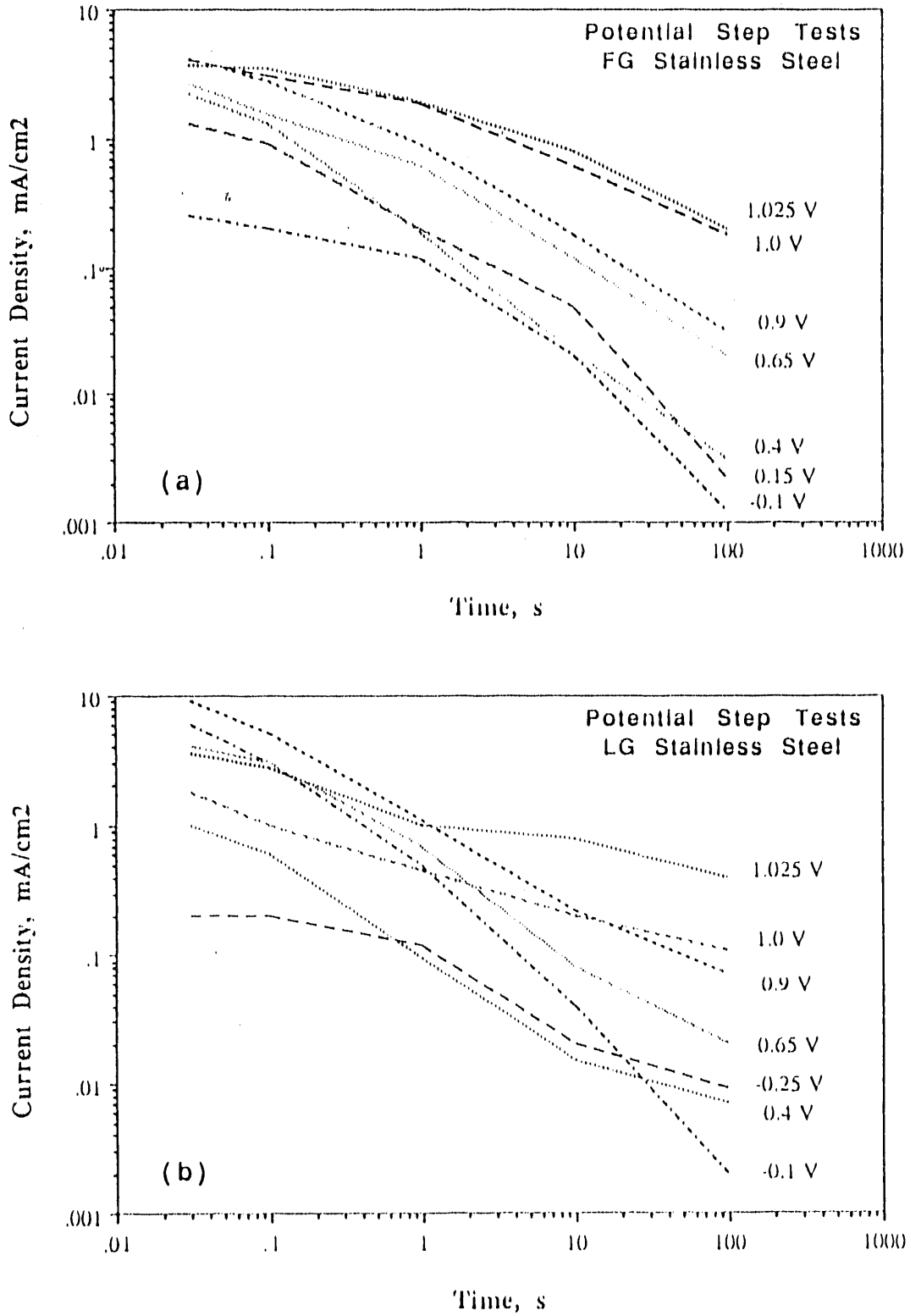

Figure 3. Potential Step Test Results for FG (a) and LG (b) Materials.

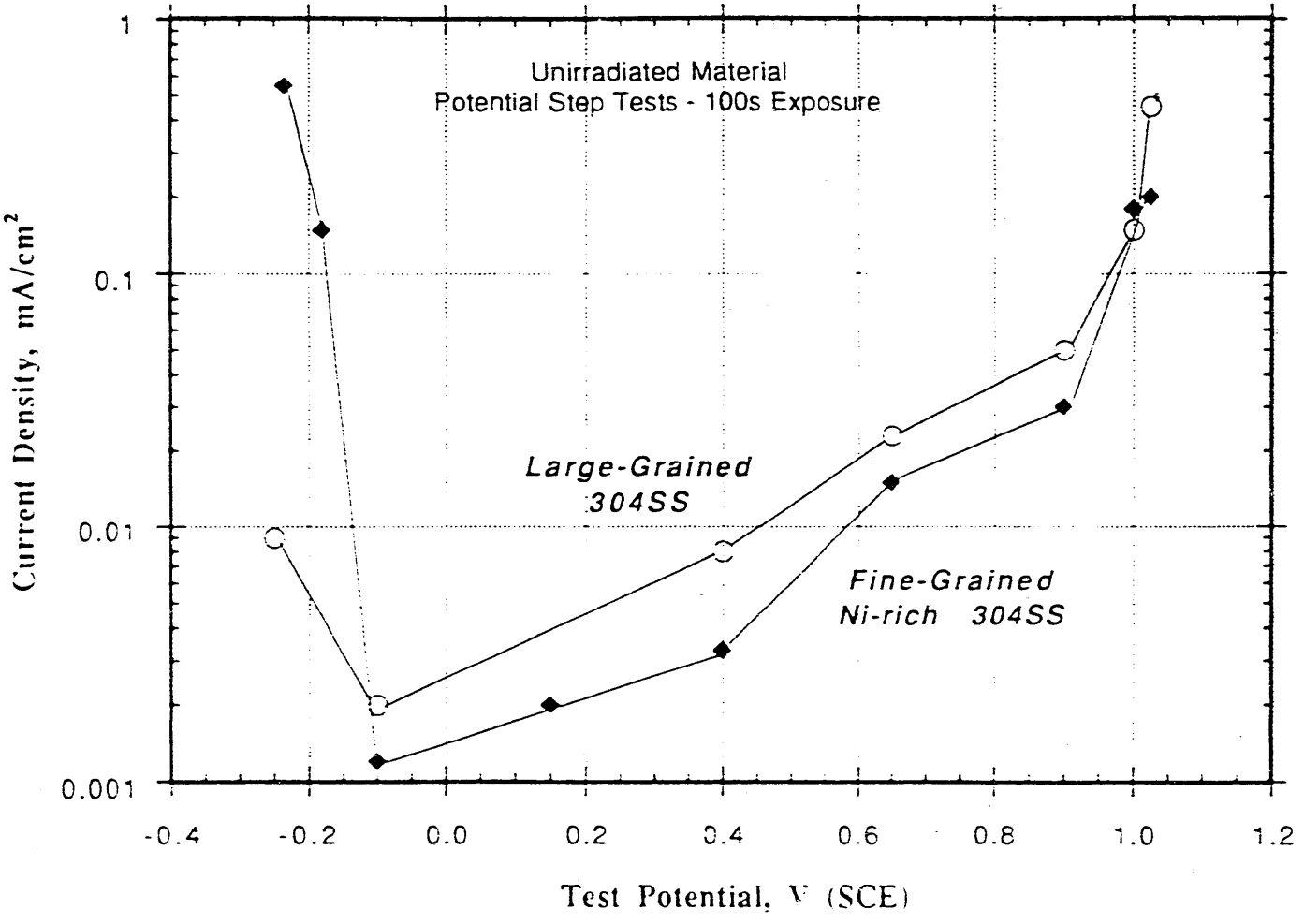

Figure 4. Current Densities after 100-s Exposures at Various Anodic Potentials.

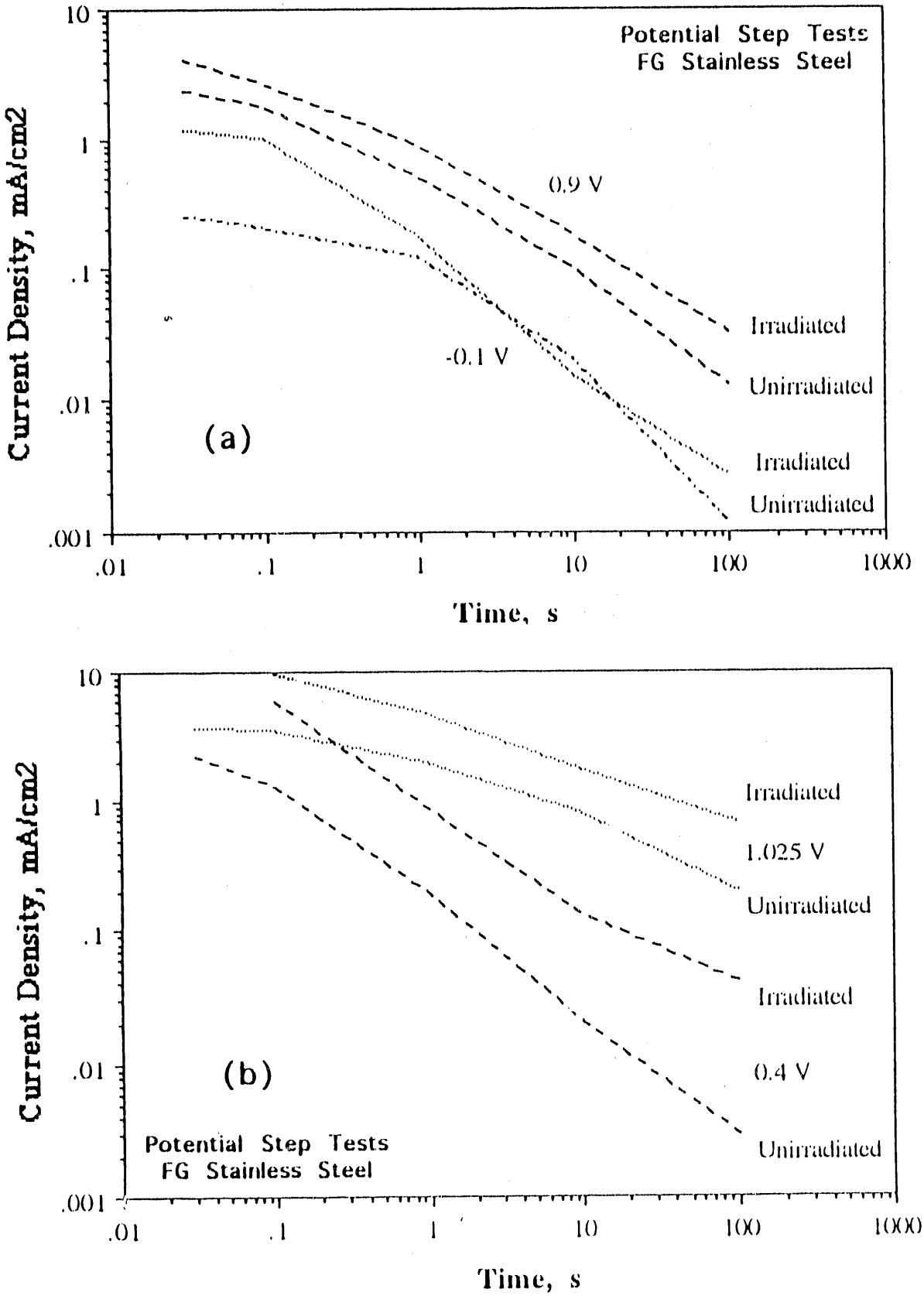

Figure 5. Comparison of Potential Step Test Results for Irradiated and Unirradiated FG Material.

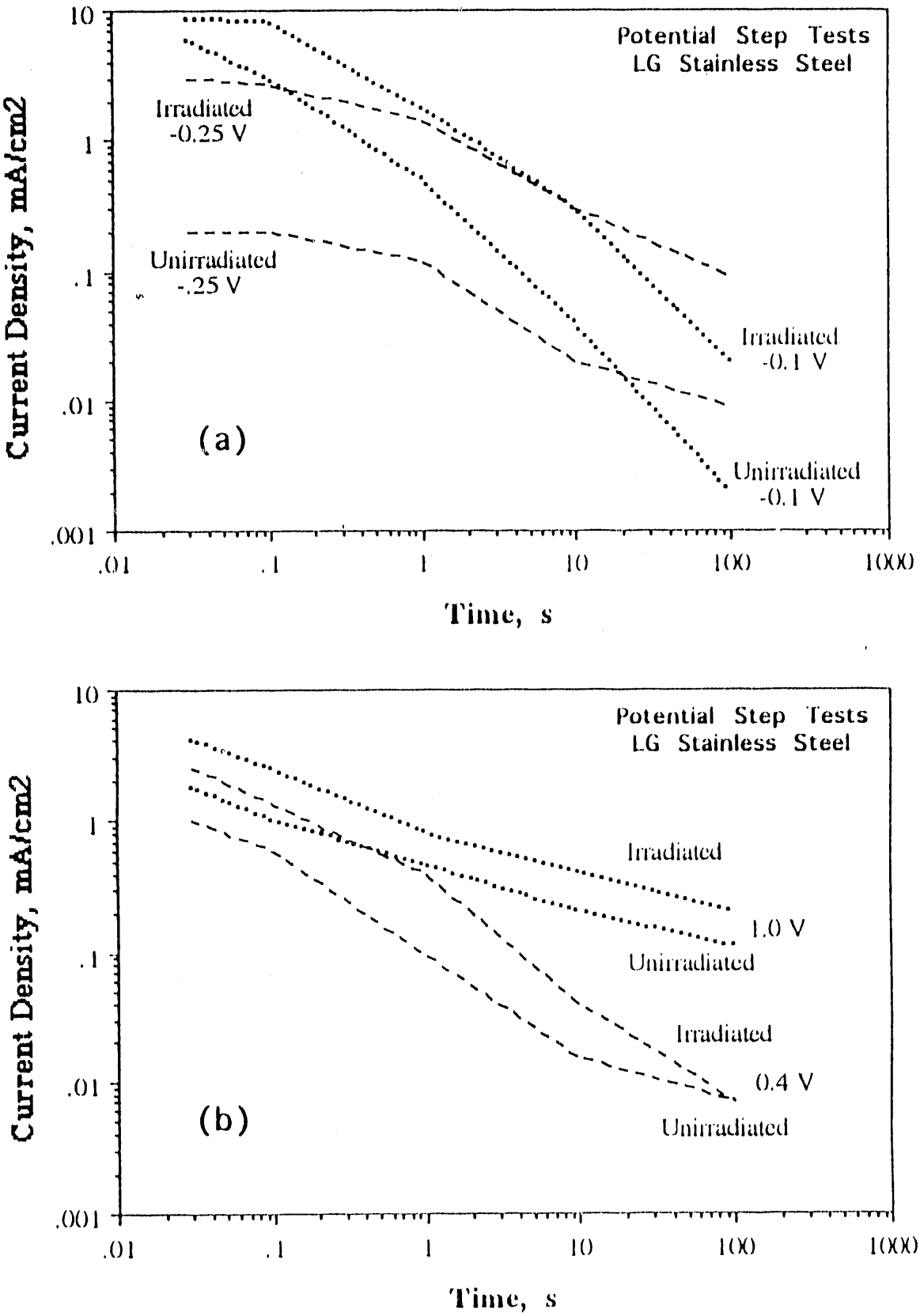

Figure 6. Comparison of Potential Step Test Results for Irradiated and Unirradiated LG Materials.

END

DATE FILMED

6/24/92